Biometric feature extraction using local fractal auto-correlation*

Chen Xi(陈 熙)[a)†] and Zhang Jia-Shu(张家树)[b)]

[a)] School of Information Engineering and Automation, Kunming University of Science and Technology, Kunming 650051, China
[b)] Key Lab of Signal & Information Processing of Sichuan Province, Southwest Jiaotong University, Chengdu 610031, China

(Received 10 October 2013; revised manuscript received 23 February 2014; published online 23 July 2014)

Image texture feature extraction is a classical means for biometric recognition. To extract effective texture feature for matching, we utilize local fractal auto-correlation to construct an effective image texture descriptor. Three main steps are involved in the proposed scheme: (i) using two-dimensional Gabor filter to extract the texture features of biometric images; (ii) calculating the local fractal dimension of Gabor feature under different orientations and scales using fractal auto-correlation algorithm; and (iii) linking the local fractal dimension of Gabor feature under different orientations and scales into a big vector for matching. Experiments and analyses show our proposed scheme is an efficient biometric feature extraction approach.

Keywords: fractal auto-correlation, fractal dimension, Gabor filter, biometric recognition

PACS: 64.60.al, 42.30.–d, 42.30.Sy **DOI:** 10.1088/1674-1056/23/9/096401

1. Introduction

Texture is an important feature of images. Texture description and analysis have been applied in the depiction of natural sceneries, such as satellite, remote sensing image recognition, biomedical image analysis, and many other fields in recent decades. There are many methods describing images' texture, such as gray-scale difference method, gray level co-occurrence matrix (GLCM) method, power spectrum method, and texture energy method.[1] Recently, fractal-dimensional image description and analysis methods have been proposed[2–5] and have been applied in many fields, such as image texture analysis,[6] surface topography analysis,[7] object recognition,[8] and classification.[9]

Fractal is proposed by Mandelbrot,[10] in which the Hausdroff–Besicovich dimension is greater than the topological dimension of mathematical set. Fractal dimension is an important element of fractal theory. Fractal dimension has been used to describe the roughness of curves or surfaces and has been applied extensively.[11–13] Pentland studied the application of three-dimensional fractal models for texture images to achieve segmentation and classification in frequency domain, and demonstrated that the fractal surface image is still fractal. The box-counting method is a widely-used approach to estimating the fractal dimension.[14,15] Based on the box-counting method, Sarkar and Chaudhuri proposed a differential box-counting method.[16,17]

In light of the fractional Brownian motion theory and its discrete form, Lundahl *et al.*[18,19] and Wen *et al.*[20] utilized the discrete Gaussian noise autocorrelation function and maximum likelihood estimation methods to estimate the fractal dimension in the spatial domain and frequency domain. Since the maximum likelihood function estimation is not explicit, seeking the maximum value of likelihood function requires massive calculation. Wang *et al.*[21] studied the relationship between the discrete Gaussian noise autocorrelation function and the distance. They also utilized the least-squares estimation method to estimate the Hurst coefficient H, and then to estimate the fractal dimension of curves or images. The estimated fractal dimension was used for classification of texture images.

In the field of biometric recognition, Li *et al.* proposed a box-counting based fractal dimension estimation approach for iris coarse classification, but they only classified the iris images into four classes.[22] Chen *et al.* utilized the fraction dimension to classify the iris images, in which the texture features of each intrinsic mode function image are obtained via the differential box-counting method.[23] Lin *et al.* proposed biometric based fractal pattern classifier for fingerprint recognition by using grey relational analysis (GRA). Subsequently, they proposed multi-fractal dimension, in which the fractal dimension was calculated by the box-counting approaches.[24] Athale *et al.* utilized fractal codes for face recognition,[25] but the calculation of pixel chaining is complex. Shang *et al.* have validated that biometric images have the characteristics of fractal, but fail to apply the fractal dimension theory to calculate the recognition rate. Furthermore, they also carried out much handwork, not completely automatically implemented by computer.[26,27]

The former fractal based biometric recognition approaches always utilized the fractal box-counting approach to

*Project supported by the National Natural Science Foundation of China (Grant Nos. 61262040, 61271341, 81360230, and 61271007) and the Applied Basic Research Projects of Yunnan Province, China (Grant No. KKSY201203062).

†Corresponding author. E-mail: xcbiometrics@126.com

© 2014 Chinese Physical Society and IOP Publishing Ltd

calculate the fractal dimensions. In this work, we use fractal auto-correlation to calculate the fractal dimensions for biometric recognition as a fractal auto-correlation is an effective image texture descriptor. In our proposed schemes, we first utilize two-dimensional Gabor filter to extract the texture feature of biometric images, and then calculate the fractal dimension of Gabor feature under different orientations and scales using fractal auto-correlation theory. Finally, we combine the fractal dimension of Gabor feature under different orientations and scales to a big vector for matching.

The rest of this paper is organized as follows. Section 2 introduces the theories about fractional Brownian motions based fractal auto-correlation. In Section 3, we address how we utilize Gabor filters and fractal auto-correlation to calculate the fractal dimension vector of biometric images. Experimental results are given in Section 4. Section 5 ends with the conclusions.

2. Fractional brownian motions based fractal auto-correlation

2.1. Fractional brownian motion model

Brownian motion was proposed by Brown in 1827, which was interpreted as the result of molecular collisions between particles. Wiener in 1923 put forward a rigorous mathematical model on Brownian motion. Mandelbrot put forward the concept of fractional Brownian motion in 1968 as follows.[28]

In the probability space, H is denoted as the index of random processes X, and satisfies

(i) $X(t)$ is continuous about t and $X(0)=0$;

(ii) for any $t \geq 0$, increment $X(t+\Delta r)-X(t)$ is Gaussian distribution with 0 mean and variance of Δr^{2H}, so the following formula will be established:

$$\begin{aligned} &P(X(t+\Delta r)-X(t)\leq x) \\ &= (2\pi)^{1/2}(\Delta r)^{-H}\int_{-\infty}^{\infty}\exp\left(\frac{-u^2}{2(\Delta r)^{2H}}\right)\mathrm{d}u, \end{aligned} \tag{1}$$

where Δr represents time increment and u is a parameter of the probability density function. According to Eq. (1), increment $X(t+\Delta r)-X(t)$ is stable and proportional to $(\Delta r)^{2H}$, so we have

$$E[X(t+\Delta r)-X(t)]^2 \infty (\Delta r)^{2H}, \tag{2}$$

where H is called the Hurst coefficient. When $H=1/2$, random processes $X(t)$ is the classical Brown motion. Falconer[29] has proved that the fractal dimension of the fractional Brownian motion curve is 2-H, and the fractal dimension of the fractional Brownian motion surface is 3-H, so the fractal dimension of texture image can be obtained by estimating H.

2.2. Discrete fractional Gaussian noise and its auto-correlation function

Supposing $B(n)$ and $B(n-m)$ are respectively discrete values of $B(t)$ at time n and $n-m$, we define the discrete fractional Gaussian noise as

$$I_m(n) = B(n)-B(n-m). \tag{3}$$

In light of Eq. (2), we have

$$E[B(n)-B(n-m)]^2 = c[n-(n-m)]^{2H}, \tag{4}$$

where c is a constant. If we incorporate Eq. (3) into Eq. (4), then

$$E[I_m(n)]^2 = c[n-(n-m)]^{2H} = cm^{2H}, \tag{5}$$

where $I_m(n)$ is a stable random process with 0 mean and $\sigma^2 m^{2H}$ variance. If $m=1$, then

$$E[I(n)]^2 = c(1)^{2H} = c. \tag{6}$$

As $\sigma^2 = E[I(n)]^2$, equation (6) can be rectified as follows:

$$c=\sigma^2, \ \text{if} \ m=1. \tag{7}$$

Supposing that $R_m(n+k,n)$ is the auto-correlation function of $I(n)$, then we have

$$R_m(n+k,n) = E[I_m(n+k)I_m(n)]. \tag{8}$$

Equation (8) can be rewritten as

$$R_m(n+k,n) = \frac{\sigma^2}{2}[(k+m)^{2H}-2k^{2H}+(k-m)^{2H}]. \tag{9}$$

We can see that there is no relationship between $R_m(n+k,n)$ and n as the auto-correlation function of the stable random process $I(n)$ has nothing to do with n, so equation (9) can be further rewritten as follows:

$$R_m(k) = \frac{\sigma^2}{2}[(k+m)^{2H}-2k^{2H}+(k-m)^{2H}]. \tag{10}$$

2.3. Auto-correlation function of digital image

Let B denote an $M\times M$ image and $B(i,j)$ the pixel value at position (i,j), where $1\leq i,j\leq M$. We suppose the difference value of two pixels with distance m can be regarded as discrete Gaussian noise, which can be calculated by the following formula:

$$\begin{aligned} I_m(i,j) &= B(i,j)-[B(i-m,j)+B(i+m,j) \\ &\quad +B(i,j-m)+B(i,j+m)]/4, \end{aligned} \tag{11}$$

where $I_m(i,j)$ is the mean Gaussian noise of $B(i,j)$ within its four neighborhoods. The auto-correlation function of discrete Gaussian noise can be calculated by

$$\begin{aligned} R(m) &= \frac{1}{M^2}\sum_{i,j=1}^{N(m)}[I_m(i,j)\times(I_m(i-m,j)+I_m(i+m,j) \\ &\quad +I_m(i,j-m)+I_m(i,j+m))/4]. \end{aligned} \tag{12}$$

2.4. Estimation of fractal dimension

From Eq. (10), we can see that there is nonlinear relationship between the auto-correlation function $R_m(k)$ of discrete Gaussian noise and the Hurst coefficient H. If $k = m$, equation (10) can be rewritten as

$$R(m) = \frac{\sigma^2}{2}[(2m)^{2H} - 2m^{2H}] = \frac{\sigma^2}{2}[2^{2H} - 2]m^{2H}. \quad (13)$$

Equation (13) is still nonlinear. If $m = 1$, we have

$$R(1) = \frac{\sigma^2}{2}(2^{2H} - 2). \quad (14)$$

Incorporating Eqs. (13) and (14), we have

$$R(m) = R(1)m^{2H}. \quad (15)$$

Performing the logarithm operation on both sides of Eq. (15), we have

$$\frac{1}{2}\log\left(\frac{R(m)}{R(1)}\right) = H\log(m). \quad (16)$$

Varying the value of m, we obtain a dot sets as follows:

$$\begin{aligned} &(\log(R(m_1)/R(1)), \log(m_1)), \\ &(\log(R(m_2)/R(1)), \log(m_2)), \\ &\qquad\vdots \\ &(\log(R(m_k)/R(1)), \log(m_k)). \end{aligned} \quad (17)$$

From Eq. (12), we can obtain the dot sets described by Eq. (17), and then utilize the least square sum approach and Eq. (16) to estimate the value of H.

3. Biometric feature extraction

3.1. Two-dimensional Gabor filter

We first adopt Gabor wavelets to obtain the matrix of the Gabor feature. The Gabor wavelets, whose kernels are similar to two-dimensional receptive field profiles of the mammalian cortical simple cells, exhibit desirable characteristics of spatial locality and orientation selectivity.[30] The Gabor wavelets can be defined as

$$\begin{aligned} \psi_{\mu,v}(z) = &\frac{\|k_{\mu,v}\|}{\sigma^2}\exp\left(-\frac{\|k_{\mu,v}\|^2\|z\|^2}{2\sigma^2}\right) \\ &\times\left[e^{ik_{\mu,v}z} - e^{-\sigma^2/2}\right], \end{aligned} \quad (18)$$

where μ and v specify the orientation and the scale of Gabor masks, respectively; $z = (x, y)$; and $\|\cdot\|$ denotes the norm operator. The wave vector $k_{\mu,v}$ is defined as: $k_{\mu,v} = k_v e^{i\varphi_\mu}$, where $k_v = k_{\max}/f^v$, and $\varphi_\mu = \pi\mu/4$. Here $k_{\max}$ is the maximum frequency, and f is the spacing factor between masks in frequency domain. The Gabor wavelet masks in Eq. (18) are all self-similar since they can be generated from one mask (filter), the mother wavelet, by scaling and rotation via the wave vector. Each mask is one of the products of a Gaussian envelop and a complex plane wave, while the first term in the bracket in Eq. (18) determines the oscillatory part of the mask and the second term compensates for the direct current value. The Gabor wavelets of five scales $\{v \in (0, 1, 2, 3, 4)\}$ and eight orientations $\{u \in (0, 1, 2, 3)\}$ are applied to represent the face image, in which $\sigma = 2\pi$, $k_{\max} = \pi/2$, and $f = \sqrt{2}$. Let $I(x, y)$ be the gray level distribution of the image. The convolution of the image $I(x, y)$ with the family of Gabor filters is defined as

$$O_{\mu,v}(z) = I(x, y)\psi_{\mu,v}(z), \quad (19)$$

where $O_{\mu,v}(z)$ is the convolution result corresponding to the Gabor kernel for an orientation μ and a scale v. The magnitudes of convolution results are used as the Gabor-represented feature matrix. Therefore, the set $S = \{|O_{\mu,v}(z)|, \mu = 0, 1, 2, 3;\ v = 0, 1, 2, 3, 4\}$ forms the Gabor wavelets representation of the image $I(x, y)$.

3.2. Extracting fractal dimension feature of biometric images

For an image, the fractal dimension is a non-integer number between 2 and 3, and it is a measure of the roughness of its intensity surface. Experiments have demonstrated that the rougher the texture appears, the larger the fractal dimension is.[31] As the area of an image is related to the roughness, to calculate the whole image's fractal dimension as the image's template is not a reasonable means. Hence, we divide the images to several sub-blocks and calculate each sub-block's fractal dimension, and then link the calculated fractal dimension with a vector for matching.

The fractal dimension of biometric images can be obtained by implementing the local fractal auto-correlation algorithm (LFAC) as follows.

1) Input training images A_i $(i = 1, 2, \ldots, M)$. Extract the Gabor magnitude feature $B^{(i)}_{\mu,v}$ of images under different orientations and scales, where i represents the i-th image, and μ and v represent the orientation and the scale, respectively.

2) Divide evenly $B^{(i)}_{\mu,v}$ into non-overlapping square sub-blocks $B^{(i)(j)}_{\mu,v}$, where $j = 1, 2, \ldots, 9$ represents the index of sub-block. Calculate the fractal dimension of $B^{(i)(j)}_{\mu,v}$ with $m_1, m_2, \ldots, m_k$ based on Eqs. (12), (16), and (17), and then obtain the fractal dimension vector of $B^{(i)(j)}_{\mu,v}$ as $F^{(i)(j)}_{\mu,v} = [F^{(i)(1)}_{\mu,v}, F^{(i)(2)}_{\mu,v}, \ldots, F^{(i)(9)}_{\mu,v}]$, where $F^{(i)(j)}_{\mu,v}$ represents the fractal dimension of $B^{(i)(j)}_{\mu,v}$.

After steps (1) and (2), we can obtain the fractal dimension vector of image A_i as

$$\begin{aligned}
F^{(i)} = [&F_{0,0}^{(i)(1)}, F_{0,0}^{(i)(2)}, \ldots, F_{0,0}^{(i)(9)},\\
&F_{0,1}^{(i)(1)}, F_{0,1}^{(i)(2)}, \ldots, F_{0,1}^{(i)(9)},\\
&F_{0,2}^{(i)(2)}, F_{0,2}^{(i)(2)}, \ldots, F_{0,2}^{(i)(9)},\\
&F_{0,3}^{(i)(1)}, F_{0,3}^{(i)(2)}, \ldots, F_{0,3}^{(i)(9)},\\
&F_{0,4}^{(i)(1)}, F_{0,4}^{(i)(2)}, \ldots, F_{0,4}^{(i)(9)},\\
&\vdots\\
&F_{3,0}^{(i)(1)}, F_{3,0}^{(i)(2)}, \ldots, F_{3,0}^{(i)(9)},\\
&F_{3,1}^{(i)(1)}, F_{3,1}^{(i)(2)}, \ldots, F_{3,1}^{(i)(9)},\\
&F_{3,2}^{(i)(2)}, F_{3,2}^{(i)(2)}, \ldots, F_{3,2}^{(i)(9)},\\
&F_{3,3}^{(i)(1)}, F_{3,3}^{(i)(2)}, \ldots, F_{3,3}^{(i)(9)},\\
&F_{3,4}^{(i)(1)}, F_{3,4}^{(i)(2)}, \ldots, F_{3,4}^{(i)(9)}].
\end{aligned} \tag{20}$$

The total dimension of $F^{(i)}$ is 180, which is used as the final biometric template for matching.

4. Experimental evaluation

In this section, we experimentally evaluate results of authentication and verification on the CAS-PEAL face database[32] and the PolyU palmprint database,[33] respectively. All the experiments were carried out on a computer with a PIV of 3.0 GHz and an RAM of 3.0 GB with Matlab 7.8. In the following experiments, m in Eq. (13) is $\{1,2,3,4,5,6,7\}$.

4.1. Database

The CAS-PEAL face database contains 99594 images of 1040 individuals (595 males and 445 females) with varying pose, expression, accessory, and lighting. The frontal face subset was used in experiments, which were collected under varying expressions (smile, frown, surprise, close eyes, and open mouth), pose, accessory, background, distance, and lighting. Some example images from the CAS-PEAL face database are shown in Fig. 1(a). The PolyU palmprint database contains 7752 grayscale images in a bitmap image format, corresponding to 386 different palms. In this database, 131 persons are male, and the age distribution is that, persons younger than 30 account for about 86 percent, persons older than 50 account for about 3 percent, and about 11 percent ages between 30 and 50. In addition, around 20 samples from each of these palms were collected in two sessions, where around 10 samples were captured in the first session and the second session, respectively. There is lighting variation in these two sessions. The average interval between the first and the second collection is 69 days. The maximum and minimum time intervals are 162 days and 4 days, respectively. The resolution of all the original palmprint images is 384×284 pixels at 75 dpi. In our paper, by using the similar preprocessing approach described in the literature,[30] the central 128×128 part of each palmprint image is cropped for further processing. Some samples in the database after preprocessing are shown in Fig. 1(b).

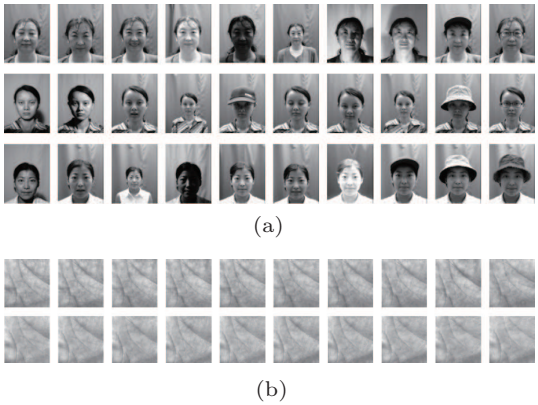


Fig. 1. (a) Sample images of three subjects from the CAS-PEAL frontal face database; and (b) twenty example palmprint images of two subjects after being cropped.

4.2. Authentication

Authentication is a one-to-many comparison against a stored training set, which answers the question of "who is the person". A testing template matches with templates stored in the central database, if the distance between the testing template and one template in the database is minimized. We think that the identity of the testing template is the same as that stored in the database. If such two templates are indeed from the same face or palm, such matching is regarded as a correct matching; otherwise, the matching is deemed as a wrong matching. In the following experiments, 100 subjects with 10 images of each subject covering pose, expression, accessory, background, distance, and lighting variation were chosen from the CAS-PEAL frontal faces database, 5 training sample images of each subject were randomly chosen for training, and the rest is for testing. The main part of each face image was cropped and resized to 112×92 pixels. Each template of testing set is matched against all templates of training set, and then we accumulate the number of correct matching. The authentication rate is the number of correct matchings divided by the number of testing samples. To further validate the efficiency of our proposed schemes in Section 3.2, we also carry out some more experiments on the palmprint database, and then compare them with the Gabor plus fractal difference box-counting approaches (FDBC) and steerable filters plus FDBC[34] in face and palmprint recognition. The difference box-counting approaches can be described as follows.[27]

A gray image can be regarded as a surface $((x,y,f(x,y))$, where $f(x,y)$ is the gray value at position (x,y). The X–Y

plane is divided into many griddings, each having a size of $L \times L$. We define $r = L/M$. At each gridding, there are several boxes with a size of $L \times L \times h$, where h is the height of one box. If the maximum gray value of the image is G, then $h = \lfloor L \times G/M \rfloor$. Supposing that the maximum gray value and the minimum gray value in the (i, j) gridding are placed at the k-th and l-th box, respectively, we have $n_r(i, j) = l - k + 1$, where $n_r(i, j)$ represents the number of box covering the (i, j) gridding. The number of boxes covering the whole image is $N_r = \sum_{i,j} n_r(i, j)$, and the fractal dimension of the whole image is then defined as

$$D = \lim \frac{\log(N_r)}{\log(1/r)}. \tag{21}$$

We can choose different L, and obtain

$$\{(L^1, N_r^1), (L^2, N_r^2), \ldots, (L^N, N_r^N)\}. \tag{22}$$

Finally, we can utilize the dot sets described by Eq. (22) and the least square sum approach to estimate the value of H.

In the experiments about palmprint authentication, 3000 images from 300 persons are chosen for experiments with 10 images of each person. We randomly choose the training samples and record the error recognition rate. We repeat the procedure 10 times and record the mean minimal error recognition rate (MMERR) and standard deviation. In the following experiments, we utilized the Euclidean metric based nearest-neighbor classifier for simplicity. Experimental results are shown in Table 1. Experimental results in the database show that the MMERR of Gabor plus LFAC is smaller than the Gabor plus FDBC with different numbers of training samples. The MMERR of the Gabor plus FDBC is smaller than steerable filters plus FDBC with different numbers of training samples, which indicates that the Gabor filters have better performance than the steerable filters on the texture description.

Table 1. MMERR (%) and standard deviation.

Method	2 train	4 train	6 train	8 train
Gabor plus LFAC (Palmprint)	3.2 ± 1.7	2.3 ± 1.9	1.7 ± 2.1	1.2 ± 2.3
Gabor plus FDBC (Palmprint)	7.3 ± 2.5	6.2 ± 2.1	5.2 ± 1.9	4.1 ± 2.2
Steerable filters plus FDBC (Palmprint)	9.6 ± 2.2	7.8 ± 1.9	6.7 ± 2.2	4.6 ± 1.8
Gabor plus LFAC (face)	18.1 ± 2.1	16.7 ± 2.6	14.2 ± 1.8	11.3 ± 1.9
Gabor plus FDBC (face)	22.3 ± 2.3	20.0 ± 2.7	17.3 ± 2.1	13.5 ± 1.8
Steer filters plus FDBC (face)	23.5 ± 2.1	21.2 ± 2.3	18.7 ± 2.2	15.6 ± 1.7

4.3. Verification

Verification is a one-to-one comparison against a stored training set, which answers the question of "whether the person is the one he claims to be". To obtain the verification accuracy of our proposed schemes, each of the testing biometric templates matches with all of the training templates stored in the central database. A matching is considered as a genuine matching if two palmprint images are from the same palm. In the following experiments, we also chose 100 subjects with 10 images of each subject covering pose, expression, accessory, background, distance, and lighting variation from the CAS-PEAL frontal faces database, 5 training sample images of each subject are randomly chosen for training, and the rest is for testing. The main part of each face image was cropped and resized to 112×92 pixels. In palmprint authentication experiments, 3000 images from 300 persons were chosen for experiments with 10 images of each person, 5 training sample images of each subject were randomly chosen to form the training set, and the rest is for testing. In the experiments on the CAS-PEAL frontal face database, the total number of matching is 250000, the number of genuine matching is 2500, and the rest are impostor matching. In the experiments on palmprint database, the total number of matching is 2250000, the number of genuine matching is 7500, and the rest are impostor matching. We plot the experimental results

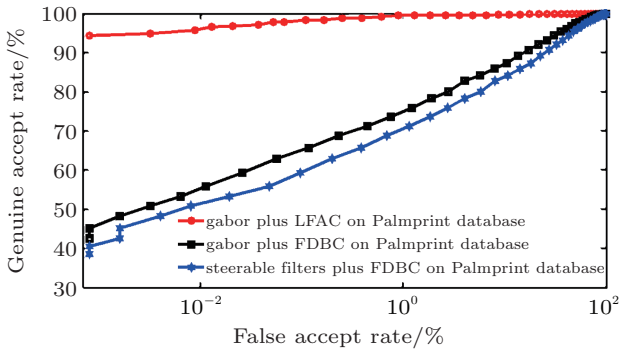


Fig. 2. (color online) The ROC curves on a subset of PolyU palmprint database.

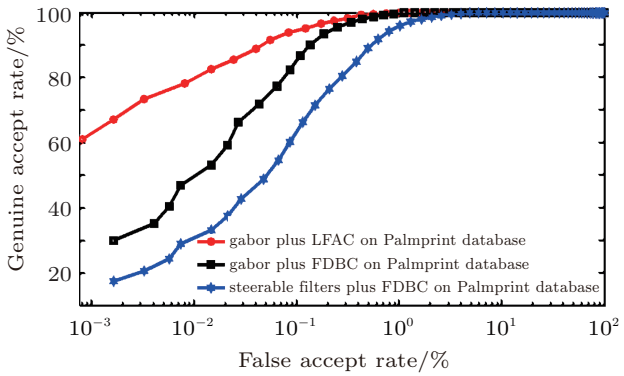


Fig. 3. The ROC curves on a subset of CAS-PEAL frontal faces database.

(genuine and impostor distribution) in Figs. 2 and 3 with a receiver operator curve (ROC). Experimental results reveal that the performance of Gabor plus LFAC is better than Gabor a receiver operator curve (ROC). Experimental results reveal that the performance of Gabor plus LFAC is better than Gabor plus FDBC, and the performance of Gabor plus FDBC is better than steerable filters plus FDBC. As the within-class variation of the face images is always larger than the between-class variation of face, and the within-class variation of palmprint images is always very little, and the verification performance on the CAS-PEAL frontal face database is worse than that on the palmprint database.

5. Complexity analysis

Multiplication is the main part of computation burden to calculate the fractal dimension in the LFAC and FDBC. Compared with the FDBC, there is extra computation in the LFAC described by Eq. (12). To calculate $R(m)$, the number of multiplication is the number of pixels in an image according to Eq. (12). In our experiments, the size of image in the CAS-PEAL database is 112×92, and the number of multiplication is $(112/3) \times (92/3) \times 9 = 10304$. In addition, we need some computation in the LFAC described by Eq. (11). In the FDBC, we should calculate $N_r = \sum_{i,j} n_r(i,j)$. However, the computation in Eq. (11) and computation in calculating N_r is little as there are mainly addition, subtraction and comparison in Eq. (11) and the computation of N_r. In the FDBC, we utilize the dot sets $\{(L^1, N_r^1), (L^2, N_r^2), \ldots, (L^N, N_r^N)\}$ and the least square sum approach to estimate the value of H. In the LFDA, we utilize the dot sets described by Eq. (17) and the least square sum approach to estimate the value of H. The computation complexity in the LFDA and FDBC to estimate H is the same.

6. Conclusion

This paper presents a local fractal auto-correlation based texture feature extraction approach of biometric images. By linking the local fractal dimension of Gabor feature under different orientations and scales to a big vector, we can obtain the effective means to classify biometric images. Experiments on the palmprint and face databases have validated the effectiveness of our proposed schemes.

References

[1] HaraIick R M 1979 *Proceedings of the IEEE* **67** 786
[2] Pentland P 1984 *IEEE Trans. Pattern Anal. Mach. Intell.* **6** 661
[3] Chaudhuri B B and Nirupam S 1995 *IEEE Trans. Pattern Anal. Mach. Intell.* **17** 72
[4] Ma Z M and Tao C K 1999 *Acta Phys. Sin.* **48** 2203 (in Chinese)
[5] Wu G H, Zhang Y J and Lin X G 2000 *J. Tsinghua University* **40** 90 (in Chinese)
[6] Wang Y N, Wang S Y and Mao J X 2006 *Journal of Hunan University* **33** 67
[7] Wu Z Q and Sun X 2001 *Acta Phys. Sin.* **50** 2126 (in Chinese)
[8] Huo Y L, Zhang G S, Lu S H and Yuan P 2013 *Acta Phys. Sin.* **62** 059201 (in Chinese)
[9] Ahn V, Yu Z G and Zhu S M 2011 *Chin. Phys. B* **20** 010505
[10] Mandelbrot B B 1982 *The Fractal Geometry of Nature* (New York: Freeman&Co)
[11] Zhang Y H,Yang Q N, Cai X J, Jiang G H and Xu X Y 2013 *Acta Phys. Sin.* **62** 080505 (in Chinese)
[12] Luo Z X, Yu H, Ping F and Ma G L 2012 *Acta Phys. Sin.* **61** 244702 (in Chinese)
[13] Kou J L, Tang X M, Zhang H Y, Lu H J, Wu F M, Xu Y S and Dong Y S 2012 *Chin. Phys. B* **21** 044701
[14] Gangepain J J and Rogues-Carmes C 1986 *Wear* **109** 119
[15] Voss R 1985 *Random Fractals: Characterization and Measurement* (New York: Plenum)
[16] Sarkar H and Chaudhuri B B 1992 *Pattern Recognition* **25** 1035
[17] Sarkar H and Chaudhuri B B 1994 *IEEE Trans. Syst. Man Cybernet.* **24** 115
[18] Lundahl T, OhIey W J, Kay S M and Siffert R 1986 *IEEE Trans. Medical Imaging* **5** 152
[19] Lundahl T, OhIey W J, Kay S M and Siffert R 1986 *SPIE Visual Communications and Image Processing* **707** 23
[20] Wen C Y and Acharya R 1998 *Pattern Recognition Lett.* **19** 735
[21] Wang H, Wang Q and Sun J W 2004 *Journal of Beijing University of Aeronautics and Astronautics* **30** 718
[22] Li Y, Zhang D, Wang K Q and Yang W 2005 *Pattern Recognition* **38** 1791
[23] Chen W K, Lee J C and Han W Y 2013 *Information Sciences* **221** 439
[24] Lin C H, Chen J L and Chiung Y T 2011 *Expert Syst. Appl.* **38** 5081
[25] Athale S S and Mitra S K 2005 *Proceedings of 2005 International Conference on Intelligent Sensing and Information* pp. 170–174
[26] Shang P J and Li T 2009 *Appl. Math. Model.* **33** 4378
[27] Li T and Shang P J A 2007 *Acta Phys. Sin.* **56** 4393 (in Chinese)
[28] Mandelbrot B B and Ness J W 1968 *SIAM Rev.* **10** 422
[29] Falconer K 2001 *Fractal Geometry: Mathematical Foundations and Applications* (translated by Zeng Wengu, Liu Shiyue, Dai Liangui) (Harbin: North East University Press)
[30] Zhang D, Kong W, You J and Wong M 2003 *IEEE Trans. Pattern Anal. Mach. Intell.* **25** 1041
[31] Asvestas P, Matsopoulos G K and Nikita K S 1999 *Pattern Recognition Lett.* **20** 347
[32] Gao W, Cao B, Shan S, Zhou D, Zhang X and Zhao D 2008 *IEEE Trans. Syst. Man Cybernet. A: Syst. Humans* **38** 149
[33] The PolyU Palmprint Database http://www4.comp.polyu.edu.hk/biometrics/
[34] Zhao Y, Gao J, Chen G and Feng W G 2011 *Chin. J. Sci. Instrum.* **29** 787